Improved Particle Confinement in Transition from Multiple-Helicity to Quasi-Single-Helicity Regimes of a Reversed-Field Pinch

L. Frassinetti,[1] I. Predebon,[2] H. Koguchi,[1] Y. Yagi,[1] Y. Hirano,[1] H. Sakakita,[1] G. Spizzo,[2] and R. B. White[3]

[1]*National Institute of Advanced Industrial Science and Technology (AIST), 1-1-1 Umezono, Tsukuba, Ibaraki 305-8568, Japan*

[2]*Consorzio RFX, Euratom-ENEA Association, Corso Stati Uniti 4, 35127 Padova, Italy*

[3]*Princeton Plasma Physics Laboratory, Post Office Box 451, Princeton, New Jersey 08543, USA*

(Received 13 September 2005; published 24 October 2006)

The quasi-single-helicity (QSH) state of a reversed-field pinch (RFP) plasma is a regime in which the RFP configuration can be sustained by a dynamo produced mainly by a single tearing mode and in which a helical structure with well-defined magnetic flux surfaces arises. In this Letter, we show that spontaneous transitions to the QSH regime enhance the particle confinement. This improvement is originated by the simultaneous and cooperative action of the increase of the magnetic island and the reduction of the magnetic stochasticity.

DOI: 10.1103/PhysRevLett.97.175001 PACS numbers: 52.55.Hc, 52.25.Fi, 52.55.Tn, 52.65.Cc

The processes of self-organization are features of many physical systems in which there is a natural evolution from a turbulent to a laminar state. An example of such systems is the reversed-field pinch (RFP) [1], a magnetic configuration for the confinement of thermonuclear fusion plasmas, which is spontaneously sustained by a dynamo process [2]. The typical RFP configuration has a safety factor profile $q(r)$ decreasing from the core to small negative values at the edge; as a consequence, a large set of magnetic modes with toroidal mode number n and poloidal mode number m satisfying the resonant condition $q(r) = m/n$, is resonant in the plasma core. In the conventional scenario, called multiple helicity (MH), the nonlinear interaction of such modes generates the dynamo field essential for the sustainment of the configuration [2], but also causes magnetic surface destruction, thus significantly deteriorating particle and energy confinement.

In the last few years, several research studies have shown that the dynamo mechanism can be produced in a regime different from MH. Theory predicts that the RFP plasma can spontaneously enter into a regime in which the dynamo is generated by a single $m = 1$ tearing mode (single helicity, SH) [3]. Under this condition the plasma core is characterized by closed helical magnetic surfaces and the conventional turbulent dynamo is replaced by a laminar dynamo with a dominant electrostatic nature [4]. Even if the SH has never been reached experimentally, regimes in which one $m = 1$ mode is dominant while the other modes (called *secondary* modes) have low amplitude, have been obtained in several RFP devices. This state, named quasi-single-helicity (QSH), has been found in all the presently working RFP experiments [5–7]; evidences of its presence were found even in old devices [8–11]. The QSH state is characterized by a global helical structure with conserved magnetic surfaces, that has been identified with the magnetic island generated by the dominant mode [5]. It is also characterized by a decrease of the secondary modes [7] and hence, in principle, by the decrease of the magnetic stochasticity throughout the core. However, to date, even if it was shown that the plasma is hotter inside the island than outside [12], there was no experimental evidence that the QSH regime can produce a better global confinement.

In this Letter, we show that QSH are regimes with improved particle confinement. In the first part of the Letter we show that spontaneous transitions from the MH regime to the QSH regime produce an enhancement of the particle confinement time, τ_p, and the growth of the soft x-ray intensity, I_{SXR}, all over the plasma. Using the experimental magnetic spectrum as input to the ORBIT code [13,14], the increase of τ_p has been verified also numerically. In the second part we discuss the physical reason for the improvement of τ_p.

Data have been taken in the TPE-RX experiment [15], an RFP device with a major radius $R = 1.72$ m and a minor radius $a = 0.45$ m. The magnetic fluctuation spectrum is measured using two toroidal arrays (placed at the inboard, and outboard sides of the vacuum vessel), each one composed of 32 coils, allowing the measurements of the edge $m = 0, 1$ fluctuations $\tilde{b}_{0,n}$ and $\tilde{b}_{1,n}$ with a toroidal number resolution up to $n = 15$. Note that the core magnetic perturbation amplitudes, in particular, the $m = 1$, are theoretically and experimentally found to be proportional to such signals [16,17]. The line-averaged electron density profile n_e is measured by a two chords (located at $r/a = 0$ and 0.69) interferometer [18] and the line-integrated alpha line emission D_α of the working gas (deuterium) is measured by a toroidal array of 17 monochromators looking at the plasma core [19]. The core electron temperature T_e, at 35 ms, is measured by a single point Thomson scattering diagnostic. All discharges analyzed are characterized by similar experimental conditions: plasma current $I_P \approx 300$ kA, reversal parameter $F = B_\phi(a)/\langle B_\phi \rangle \approx -0.1$, pinch parameter $\Theta = B_\theta(a)/\langle B_\phi \rangle \approx 1.4$, and electron density $n_e \approx 6 \times 10^{18}$ m^{-3}.

In TPE-RX both long-lasting QSH and intermittent QSH are commonly found [7]. Figure 1 shows an example of intermittent QSH. The increase of the dominant mode $b_{1,n=6}$, the innermost resonant one, goes with the reduction of the secondary modes, Fig. 1(b). The shape of the magnetic fluctuations can be quantitatively estimated analyzing the spectral index, $N_s = [\sum_n (\tilde{b}^2_{1,n}/\sum_n \tilde{b}^2_{1,n})^2]^{-1}$; a pure SH regime corresponds to $N_s = 1$, while the QSH regime, having residual secondary modes, has $N_s > 1$. To discriminate between QSH and MH, we choose the threshold value $N_s = 3$ [7]. The time evolution of N_s is shown in Fig. 1(c); during the discharge, several transitions from MH to QSH occur. The I_{SXR} signal measured by a central chord divided by n_e^2 is shown in Fig. 1(d), along with the total radiation P_{rad}. I_{SXR}/n_e^2 is related to impurities and to T_e [$I_{\mathrm{SXR}}/n_e^2 \propto f(Z_{\mathrm{eff}})T_e^{\gamma}$ with $\gamma \approx 3$ in TPE-RX] and is well correlated with N_s; on the contrary P_{rad} is related mainly to impurities and is not correlated with N_s. We cannot completely exclude a contribution due to the impurities, but these results, supported by the trend between T_e and N_s in Fig. 5(b), indicate that the main contribution to the enhancement of I_{SXR}/n_e^2 is due to the T_e term. Note that, even if I_{SXR} decreases after 40 ms due to the waveform of I_P, Fig. 1(a), the transition to the QSH state still produces the increase in I_{SXR}/n_e^2, at $t \approx 51$ ms. Moreover, the I_{SXR}/n_e^2 enhancement occurs throughout the plasma and not only inside the magnetic island; this is shown by the radial profiles of Fig. 1(e) calculated at $t_1 \approx 32.2$ ms and at $t_2 \approx 33.7$ ms that are the time from which the plasma begins the transition to the QSH regime and the time of the purest QSH. Figure 2, which shows the tomographic SXR images at t_1 and t_2, confirms that the magnetic island characterizes the plasma core during QSH states.

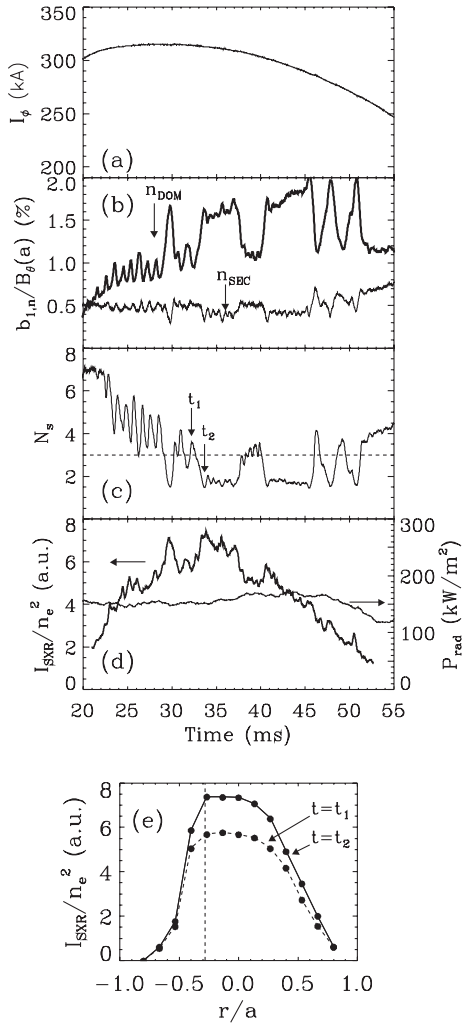

FIG. 1. Example of intermittent QSH: time evolutions of (a) plasma current, (b) dominant mode, and root mean square of secondary modes, (c) N_s and (d) I_{SXR}/n_e^2, and total radiation P_{rad} measured by the central chord of the bolometer. Frame (e) shows the radial profile of I_{SXR}/n_e^2 at t_1 during MH and at t_2 during the QSH regime. The vertical dashed line represents the radial position of the island.

Transitions from the MH to QSH regimes produce the improvement of the particle confinement time τ_p. The latter has been calculated using the relation $\tau_p = N_e/(C\langle D_\alpha\rangle - dN_e/dt)$, where N_e is the total number of particles determined from density measurements, $\langle D_\alpha\rangle$ is the toroidally integrated D_α emission, and C is a constant determined as in Ref. [18]; note that the source term is proportional to the D_α emission, see Ref. [18]. The core density and the peaking factor $P = n_e^{\mathrm{core}}/n_e^{\mathrm{edge}}$ are shown in Fig. 3(a) and $\langle D_\alpha\rangle$ in Fig. 3(b). During the MH-QSH transition the density is almost constant, supporting the idea of a continuos MH-SH transition, being QSH an intermediate stage that does not require (up to the present knowledge) a drastic change of profiles. Nevertheless, the reduction of the source term shows that the transport has to be reduced and hence that τ_p has to be increased, Fig. 3(c). In the last part of the discharge, at ≈ 48 ms and ≈ 51 ms, the transitions do not produce a clear increase of τ_p; this is due to the relatively high level of secondary modes that decrease only to ≈ 0.4, Fig. 1(b), while they decrease up to 0.3 in the earlier transitions. As described below, τ_p depends on the amplitude of the secondary modes as well as of the dominant one.

The improvement of τ_p in the QSH regime has been verified also numerically, using the Hamiltonian guiding center code ORBIT [13]. To confirm the performance im-

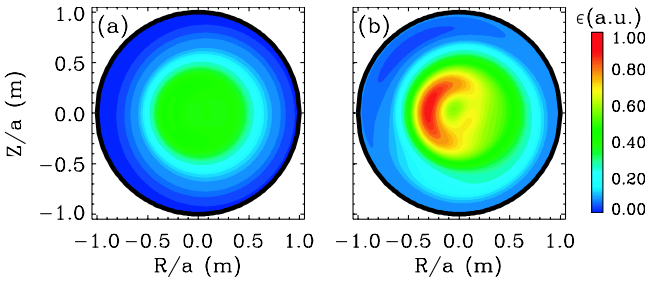

FIG. 2 (color online). Tomographic SXR images at (a) t_1 during the MH state and (b) t_2 during the QSH state.

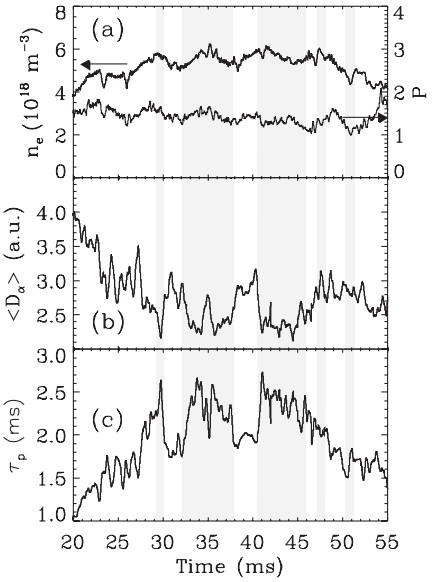

FIG. 3. Time evolutions of (a) core electron density n_e and peaking factor P, (b) integrated D_α radiation, (c) particle confinement time τ_p. Gray areas highlight the QSH states.

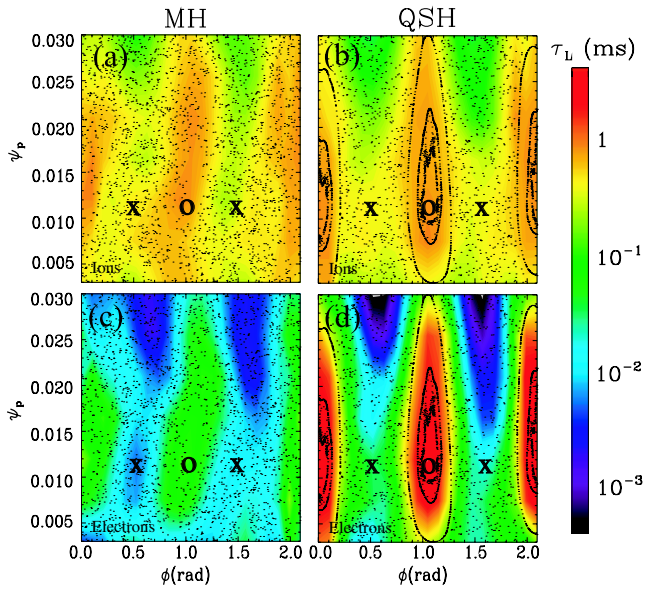

FIG. 4 (color online). Poincaré sections of the magnetic fields (black points) in the MH (a),(c) and QSH (b),(d) cases. Overplotted, as a colored contour, the values of the loss time τ_L for ions (a),(b) and electrons (c),(d).

provement in the MH to the QSH transition, experimental data of the same shot of Fig. 3, at t_1 (hereafter called the MH case) and t_2 (hereafter called the QSH case), have been used as inputs for the code. Typical TPE-RX thermal conditions, energies $T_i \sim 300$ eV and $T_e \sim 550$ eV and collision frequencies $\nu_i \sim 2.7 \times 10^3$ sec^{-1} and $\nu_e \sim 3.6 \times 10^5$ sec^{-1} have been adopted; magnetic data at the plasma edge are taken into account, solving the equilibrium magnetic field and the (pressureless) Newcomb equation for the perturbations; the latter procedure involves the experimental measurements of both the radial b_r and toroidal b_ϕ components of the fluctuations at the edge. Transport properties are deduced by the time τ_L required to lose 50% of the particles deposited in the plasma core out from a preset border located at an outer radius [14]. For the present investigation a set of particles, with random pitch, $v_\parallel/v$, distribution in the interval $[-1, +1]$, has been deposited on the vertices of a dense mesh on the $\theta = 0$ plane, varying the radial and the toroidal coordinates (ψ_p, ϕ) only, where ψ_p is the poloidal flux coordinate and ϕ is the toroidal angle [13]. The results are shown in Fig. 4. In the four frames the toroidal section of the Poincaré map (black dots) and τ_L (in every position, the color represents the loss time for the set of particles therein deposited) are shown. While in the MH case [Figs. 4(a) and 4(c)] the field is mostly stochastic, in the QSH case [Figs. 4(b) and 4(d)] clear conserved magnetic surfaces emerge, corresponding to a $(m, n) = (1, 6)$ magnetic island. Concerning ion loss time τ_L^i, the comparison between MH and QSH is shown in Figs. 4(a) and 4(b); τ_L^i has the same trend in both cases: ion transport is not markedly affected by the presence of the QSH island, but at the same time the MH case seems to retain a helical perturbation (the reason will be discussed later); the relatively large collisional effects together with the toroidal drift tend to smooth out the macroscopic magnetic structures. Instead, as far as electrons are concerned, such effects are significantly smaller: the loss time τ_L^e is strongly affected by the conserved flux surfaces, as shown in Figs. 4(c) and 4(d), but an increase of confinement, with respect to the MH case, exists not only inside the island. To better quantify the latter point, we can consider the values of $\tau_L^{i/e}$ averaged on small portions surrounding the best or worst transport performance locations in the core, i.e., the island O point (indicated in the figure with O) and the point at the same radial position in antiphase to it (indicated with X). The results are summarized in Table I. As pointed out in Ref. [14], we expect the transport to be mainly determined by the slowest species, therefore a qualitative behavior for ambipolar transport can be deduced. Regarding the O region, in MH, ions drive the ambipolar transport $[\tau_L^i(O)/\tau_L^e(O) \sim 10]$, whereas in QSH, the transport is led by electron motion $[\tau_L^i(O)/\tau_L^e(O) \sim 1/2]$, with a resulting improvement in ambipolar confinement inside the island. In the X region, the MH case shows a purely stochastic behavior, with a ratio $\tau_L^i(X)/\tau_L^e(X) \sim 20$–$40$ and a consequent ambipolar loss time expected to be $\tau_L^a(X) \sim \tau_L^i(X)/2$; see [14]. Conversely, QSH shows a decrease in stochasticity as the ratio between the loss times is lower, $\tau_L^i(X)/\tau_L^e(X) \lesssim 10$. As a consequence, for the latter case we expect in the X region an ambipolar time $\tau_L^a(X)$ larger than $\tau_L^i(X)/2$. These assertions on the extreme values of τ_L^a, together with the realization that in the MH case the loss times of the X region match a wide part of the plasma core performances [where therefore we can consider $\tau_L^a \sim \tau_L^i(X)/2$], allow us

TABLE I. Average τ_L in the MH and QSH cases.

τ_L (ms)	MH	QSH
$\tau_L^i(O)$	0.6 ± 0.2	1.0 ± 0.2
$\tau_L^e(O)$	0.06 ± 0.01	2.2 ± 0.2
$\tau_L^i(X)$	0.5 ± 0.2	0.5 ± 0.2
$\tau_L^e(X)$	0.02 ± 0.01	0.08 ± 0.01

to deduce a global particle confinement improvement in the core for QSH, even though a direct ambipolar loss time computation is not possible, due to the coexistence of stochastic and regular zones [14]. When we consider the outer region, the two cases, QSH and MH, become approximately equivalent. Here we should highlight that in the MH case ($t = t_1$) $\tilde{b}_{1,6}$ is still more than the double of $\tilde{b}_{1,\mathrm{sec}}$, Fig. 1(b), explaining the surviving asymmetric behavior of τ_L in Figs. 4(a) and 4(c). Using experimental data of purer MH regimes, even more conclusive results have been obtained.

A statistical study has been performed over an ensemble of shots under the same experimental conditions. Data have been sampled in time intervals 1 ms long, between 25–35 ms, i.e., only during the flat top of the discharge. The trend of τ_p versus N_s is shown in Fig. 5(a). The increase of τ_p with the decrease of N_s shows that approaching the purest QSH regimes the particle confinement is improved. The same trend has been found for T_e versus N_s, Fig. 5(b), showing that the QSH plasma is hotter than the MH plasma.

The parameter N_s contains information on the shape of the whole magnetic spectrum; separating the contribution of dominant and secondary modes allows us to get insight into the real cause of the confinement improvement. In Fig. 5(c) we show the trend of τ_p versus the dominant mode, $\tilde{b}_{1,6}$. The MH regime is not affected by $\tilde{b}_{1,6}$, instead, in QSH regimes τ_p increases with $\tilde{b}_{1,6}$. The increasing of the amplitude of $\tilde{b}_{1,6}$ helps the emergence of extended regions with well-conserved flux surfaces, which locally increase the particle confinement. Also the decrease of the secondary modes play a crucial role for particle confinement: due to the related reduction of the magnetic field stochasticity outside the island, τ_p clearly scales with $\tilde{b}_{1,\mathrm{sec}}$ [Fig. 5(d)]. The improved confinement is therefore due to the cooperative effect of the reduction of the secondary modes and of the increase of the dominant mode.

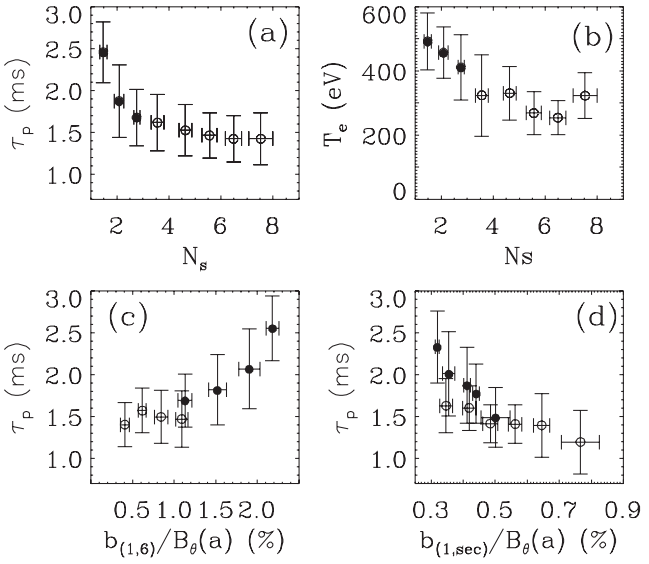

FIG. 5. Correlations of (a) τ_p and (b) T_e versus N_s. Correlation of τ_p versus (c) the dominant mode and (d) the rms of the secondary modes for MH (○) and QSH (●).

In this Letter we have shown that spontaneous MH to QSH transitions bring a global improvement of particle confinement. Furthermore, a global higher energy confinement is suggested by both the increase of I_{SXR}/n_e^2 and the trend of T_e vs N_s, which show a higher core electron temperature.

The authors are grateful to L. Marrelli and L. Carraro for useful discussions. This work was financially supported by the Budget for Nuclear Research of the Ministry of Education, Culture, Sports, Science and Technology of Japan based on screening and counseling by the Atomic Energy Commission, by European Communities under the contract of Association between EURATOM/ENEA, and by the U.S. Department of Energy Grant No. DE-FG03-94ER54271.

[1] H. A. B. Bodin and A. A. Newton, Nucl. Fusion **20**, 1255 (1980).
[2] S. Ortolani and D. D. Schnack, *Magnetohydrodynamics of Plasma Relaxation* (World Scientific, Singapore, 1993).
[3] S. Cappello and D. F. Escande, Phys. Rev. Lett. **85**, 3838 (2000).
[4] D. Bonfiglio, S. Cappello, and D. F. Escande, Phys. Rev. Lett. **94**, 145001 (2005).
[5] P. Martin *et al.*, Nucl. Fusion **43**, 1855 (2003).
[6] L. Marrelli *et al.*, Phys. Plasmas **9**, 2868 (2002).
[7] P. Piovesan *et al.*, Phys. Plasmas **11**, 151 (2004).
[8] G. A. Wurden, Phys. Fluids **27**, 551 (1984).
[9] R. J. Hayden and B. Alper, Plasma Phys. Controlled Fusion **31**, 193 (1989).
[10] P. R. Brunsell *et al.*, Phys. Fluids B **5**, 885 (1993).
[11] P. Nordlund and S. Mazur, Phys. Plasmas **1**, 4032 (1994).
[12] D. F. Escande *et al.*, Phys. Rev. Lett. **85**, 1662 (2000).
[13] R. B. White and M. S. Chance, Phys. Fluids **27**, 2455 (1984).
[14] I. Predebon *et al.*, Phys. Rev. Lett. **93**, 145001 (2004).
[15] Y. Yagi *et al.*, Fusion Eng. Des. **45**, 409 (1999).
[16] P. Zanca and F. Sattin, Plasma Phys. Controlled Fusion **45**, 1 (2003).
[17] D. Brotherton-Ratcliffe, C. G. Gimble, and I. H. Hutchinson, Plasma Phys. Controlled Fusion **29**, 161 (1987).
[18] A. Canton *et al.*, Plasma Phys. Controlled Fusion **46**, 23 (2004).
[19] Y. Yagi *et al.*, Rev. Sci. Instrum. **74**, 1563 (2003).